DEVELOPMENT OF AN MR-COMPATIBLE SPECT SYSTEM BASED ON ENERGY RESOLVED PHOTON COUNTING DETECTORS

BY

LIANG CAI

THESIS

Submitted in partial fulfillment of the requirements
for the degree of Master of Science in Nuclear, Plasma and Radiological Engineering
in the Graduate College of the
University of Illinois at Urbana-Champaign, 2010

Urbana, Illinois

Master's Committee:

Professor Ling-Jian Meng, Chair
Professor James F. Stubbins

DEVELOPMENT OF AN MR-COMPATIBLE SPECT SYSTEM BASED ON ENERGY RESOLVED PHOTON COUNTING DETECTORS

Liang Cai, M. S.
Nuclear, Plasma and Radiological Engineering
University of Illinois at Urbana-Champaign, 2010
Ling-Jian Meng, Advisor

Nuclear medicine is playing an important role in the clinical diagnosis and therapy. Single Photon Emission Computed Tomography (SPECT) is one of the most important nuclear imaging modalities, and it gives the functional imaging of the region of interest. MR can provide the anatomical imaging and enjoys better soft tissue contrast comparing to Computed Tomography. In this thesis, a MR compatible SPECT system is developed and the performance of this system is evaluated. This SPECT system is based on novel energy-resolved photon counting (ERPC) detectors we have recently developed for gamma ray imaging applications. The ERPC detector has basic modular configuration that offers an overall detection area of 4.5 cm×4.5 cm, comprising of eight CdTe/CMOS detector hybrids. Each hybrid has a CdTe detector of 11 mm×22 mm bump-bonded onto a dedicated readout ASIC that has 32×64 readout pixels with 350μm pitch size. The 1mm and 2mm thickness CdTe detector have both been developed. This configuration offers a very-high spatial resolution of around 350μm and an excellent energy resolution of around 3~4 keV at 140 keV. The prototype SPECT system that consists of two or four ERPC detectors is mounted on a system gantry rotating around a horizontal axis. The detectors are coupled to apertures with differently sized pinholes. In order to utilize the imaging information provided by the ERPC detector, we have developed a comprehensive system modeling and calibration method that accounts for the irregular shapes and physical details in the collimation apertures. Besides this, a detailed charge collection inside strong magnetic field is developed by J.W Tan in our group, and a MR correction model based on this model is used to reconstruct SPECT image inside strong magnetic field. Detailed system design and experimental procedures will be described in this thesis.

Keywords: MR-SPECT; Energy resolved photon counting detector; Geometry calibration; Image reconstruction

TABLE OF CONTENTS

CHAPTER 1. INTRODUCTION

In recent years, multi-modality imaging techniques are becoming more and more important. Among these modalities, combined magnetic resonance imaging (MRI) and nuclear imaging techniques, such as MRI/PET and MRI/SPECT, have shown a great potential [1-6]. The MRI could provide the anatomical image of the particular organs, tissues or cells, and these nuclear imaging techniques are capable of following functional metabolism and physiology of them. Compared to conventional X-ray CT, MRI provides a much better soft tissue contrast. At the same time, the rapidly changing field of molecular imaging has led to substantial efforts for developing a wide variety of imaging techniques dedicated to small animal studies [7]. Amongst commonly used imaging modalities, dedicated positron emission tomography (PET) and single photon emission computed tomography (SPECT) permit in vivo assessment of distribution of radiolabeled molecules in small animals. PET does not require physical collimation and therefore offers a sensitivity that is typically 1 or 2 orders of magnitude higher than the typical sensitivities of SPECT systems. On the other hand, SPECT requires a simpler detection system, which could (potentially) offer a superior spatial resolution and enjoy a wide range of radiotracers that are readily available commercially. Most of the recent efforts on SPECT instrumentations could fall into the following three categories. Firstly, a tremendous amount of efforts have been devoted to improve the spatial resolution of SPECT systems, especially for imaging small lab animals. This improvement is mainly coming from the use of gamma ray sensors with an excellent intrinsic spatial resolution [8-11] and the use of focusing geometries that have relatively large magnification ratios. Secondly, many research teams have been exploring various aperture designs that

improve raw sensitivity by introducing a controlled amount of multiplexing in projection data. Thirdly, several recent efforts started to target at the so-called adaptive SPECT imaging [12]. In this approach, the SPECT hardware can be modified, adaptively in real time, to offer an optimal efficiency for collecting useful imaging information regarding the particular object being studied.

In this thesis, we report the preliminary performance of a very-high resolution SPECT system based on recently developed energy-resolved photon-counting (ERPC) CdTe detectors. The ERPC detector is designed to offer a high spatial resolution, a wide dynamic range of 12-200 keV and an excellent energy resolution of around 3~4 keV. In order to evaluate the use of the ERPC detector for various SPECT applications, we have constructed a prototype SPECT system that consists of two or four ERPC detectors supported on a horizontally mounted rotational gantry. In this study, we have carried out a series of experimental studies to evaluate the intrinsic performance of the ERPC detector and the imaging capability of the prototype MR compatible SPECT system. The results from these studies will be presented in this thesis.

CHAPTER 2. SYSTEM DEVELOPMENT

2.1 Energy-resolved photon-counting (ERPC) CdTe detector

The SPECT system is based on the recently developed Energy Resolved Photon-Counting (ERPC) detectors [13]. The ERPC detector (Fig.1.) consists of multiple CdTe detectors that are flip-chip bonded onto a newly developed readout ASIC. The ASIC is realized through a mixed signal, 4 metal 2 poly CMOS process based on commercial 350 nm technology. The overall dimensions of the ASIC are approximately 22 mm×11 mm, accommodating a total of 2048 readout channels arranged in an array of 32×64 pixels (Fig.2). The pixel pitch size is 0.35 mm × 0.35 mm, which matches the pixel configuration of the CdZnTe or CdTe detectors in use. Each CMOS pixel has a bump-bonding pad of 25 μm in diameter. The pixel readout circuitry includes an AC-coupled charge-sensitive amplifier, a peak-hold (P/H) circuit,

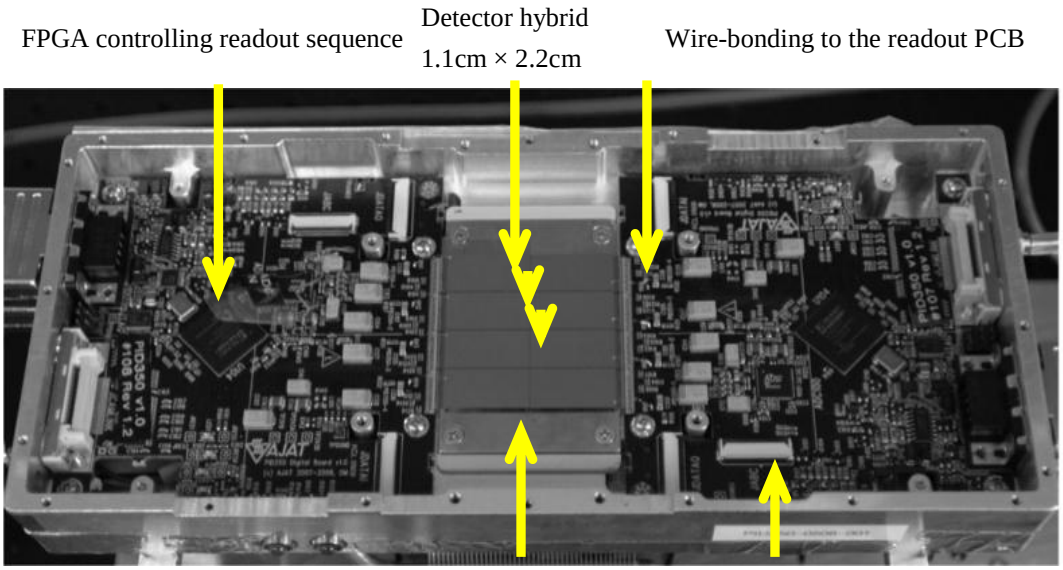

Fig.1. The prototype ERPC CdTe detector

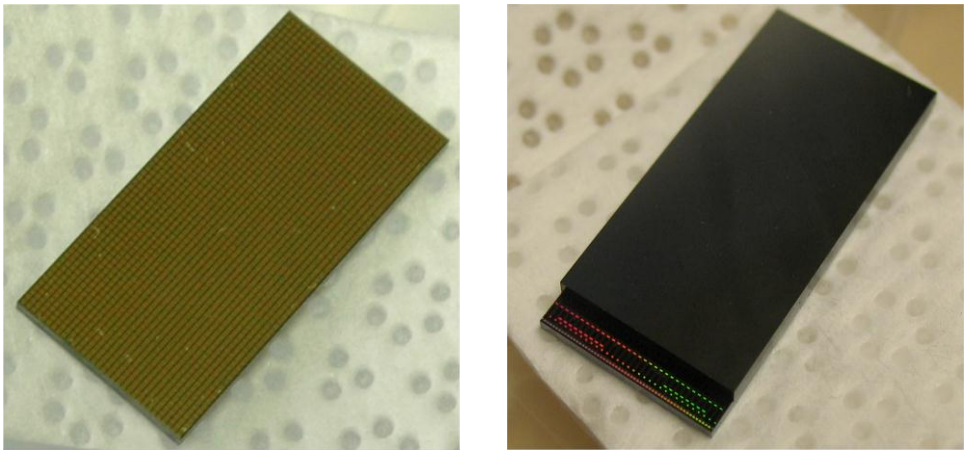

Fig.2 (Left) Image of a 0.1×2×2 cm3 CdTe detector with 350 μm pixels.
(Right) A CdTe/ASIC hybrid.

a comparator and a multi-function counter used for both photon counting and A-to-D conversion. The pixel circuitry also contains various logic units for controlling, address decoding, and selection between readout modes. The amplifier has a shaping time of ~1 μs. The comparator in each pixel has a typical differential topology that uses an external analog control voltage to adjust the threshold level. All the wire-bonding pads, including the control signals, power feeds, and output signals, are located on one side of the ASIC. In order to compensate for the pixel-to-pixel variations in the channel offset and gain, each channel is also equipped with two 8-bit digital-to-analog converters (DACs). These allow accurate alignment of the readout channels on the detector.

One of the key features of the ERPC ASIC is the capability to perform on-pixel A-to-D conversion with variable precision. Following an interaction in the detector, the trigger signal from an anode pixel is used to initiate a time-to-digital converter (TDC) located on the same pixel. At the same time, the triggering signal is also used to start a ramp generator. The ramp

generator is implemented using an 8-bit digital-to-analog converter (DAC) that is driven by a clock signal operating at 10 MHz. The ramp generator outputs a steadily increasing ramp signal that is compared with the signal amplitude held by the on-pixel P/H circuitry. When these two amplitudes are sufficiently close to each other, a trigger signal is generated to stop the TDC. Therefore, the output of the TDC is proportional to the signal amplitude induced on the corresponding anode pixel. Depending on the desired count rate capability, the analog signal can in principle be digitized with different precision by changing the step size of the ramp generator. For each event, it takes a maximum of <10 μs to perform a 6-bit A-to-D conversion and around 25.6 μs for an 8-bit conversion. After the A-to-D conversion, the pixel address and the digital amplitude are sent out, and the ASIC is reset to receive future incoming events. Using this readout mode, each ASIC is in principle capable of handling 0.1 M counts per second (cps) with 6-bit ADC precision and 25 kcps with 8-bit precision. If necessary, the eight ASICs on each ERPC detector can be designed to operate independently. Therefore, the entire ERPC detector is capable of a count rate of 0.2 Mcps with 6 bit ADC precision. For high resolution SPECT imaging, the event rate exposed to gamma ray detectors is generally limited by the use of high-resolution collimation apertures. Therefore, the count rate of the ERPC detector should be more than adequate for most high-resolution SPECT applications.

The hybrids are wire-bonded to readout printed circuit boards (PCBs) as shown in Fig. 1. These PCBs provide the power feed, logic and timing signals, and data pathway for the ASICs. Each readout board also has a 32 MB data buffer for temporary storage of pixel addresses and digital signal amplitudes. The readout operation of the camera is controlled by

FPGAs mounted on the digital boards, which act as a bridge between the ERPC ASICs and the control software. For the ERPC detector, a universal threshold is used for all readout channels. The threshold level is controlled by an 8-bit DAC located on the readout board. The selectable threshold level has a resolution corresponding to 0.46 keV. The eight ASICs are mounted onto a copper back-plate that is attached to a Peltier cooling unit for heat dissipation.

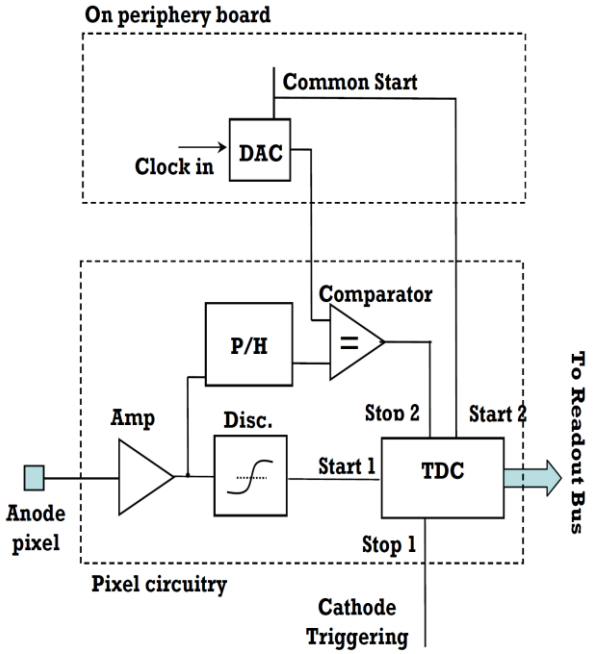

Basic pixel circuitry

Fig.3. The pixel circuitry consists of pre-amp, shaping-amp, discriminator, peak-hold units. The signal amplitude is digitized with an on-pixel ADC that works based on counting the time required for a steadily increasing ramp signal to reach the P/H amplitude.

The digital PCBs are connected to the host PC through either USB 2.0 or CameraLink interfaces. The pixel circuitry of this detector is shown on Fig.3.

2.2 MR compatible SPECT system based on ERPC detectors

The prototype SPECT system used in this study is shown in Fig. 4. Two or four camera heads are supported on a gantry rotating around a horizontal axis at arbitrarily chosen angular steps. The gantry is driven by a Velmax rotary stage with an encoder having an angular precision of 0.01 degree. The distance between the detector surface and the rotation axis is designed to be around 7 cm. Each detector head is coupled to a multiple pinhole aperture that has 9 pinholes arranged in 3×3 pattern. The distance between nearest pinholes is around 7 mm, but the actual pinhole position was randomly moved around the grid point to avoid

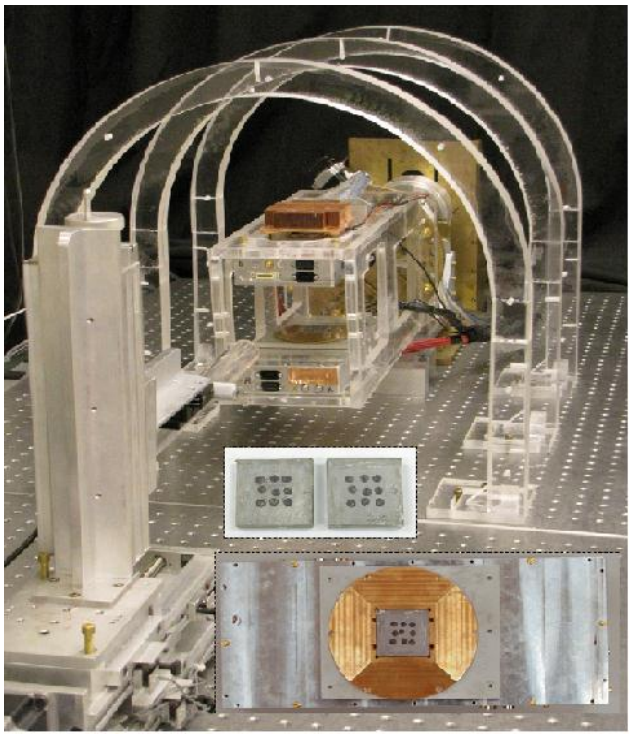

Fig.4. Two cameras are supported on the rotary gantry, the collimation apertures and how they are mounted on the detectors are also shown.

oversampling at certain discrete spatial frequencies. The body of the aperture is made of lead sheet of 8 mm thickness. It has nine through holes, each with a pinhole-insert fitted inside.

All pinholes in the aperture are pointing towards a focal spot that is 3.5 cm from the center-plane of the aperture. The pinhole inserts are made of pure tungsten. They are 6 mm tall and have an acceptance angle of 60 degrees on both sides. The diameters of the pinholes are ranging from 200 μm to 400 μm diameter. The center axial section of the pinholes has a channel of 100 μm length. The fact that the pinhole inserts are 2 mm shorter than the thickness of the lead sheet and all pinholes are pointing to a focal spot give rise to a complicated pinhole geometry that needs to be modeled precisely for an accurate geometrical calibration and reconstruction. The aperture photo and the mounting configuration is also shown in Fig. 4.

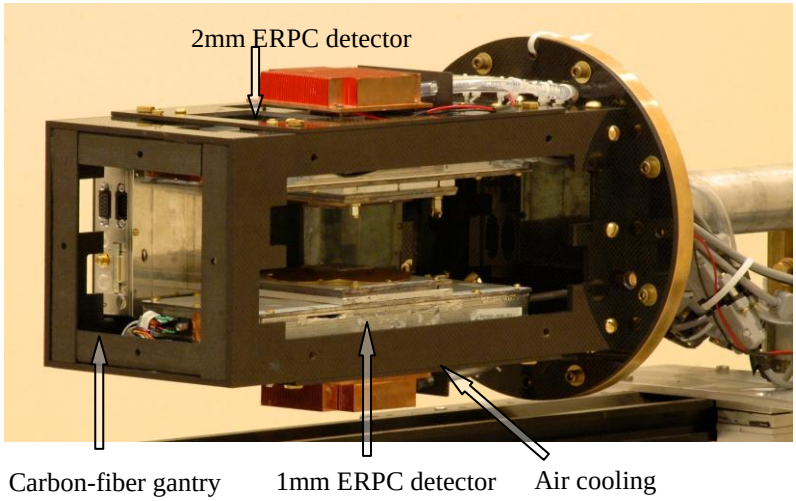

Fig. 5. Four-head SPECT system based on ERPC CdTe detectors, the gantry is made of carbon-fiber materials to achieve better geometry stability

To make the gantry more stable for accurate imaging study, a carbon-fiber gantry is fabricated to support the camera heads. In this new supporting gantry, the distance between the rotating axis and the aperture can also be adjusted. Four detectors can be mounted on this gantry as shown on Fig. 5. The gantry and all the components of the system are MR

compatible. The whole SPECT system can be settled on a compact portable cart which can be easily used in the MR room (Fig. 6).

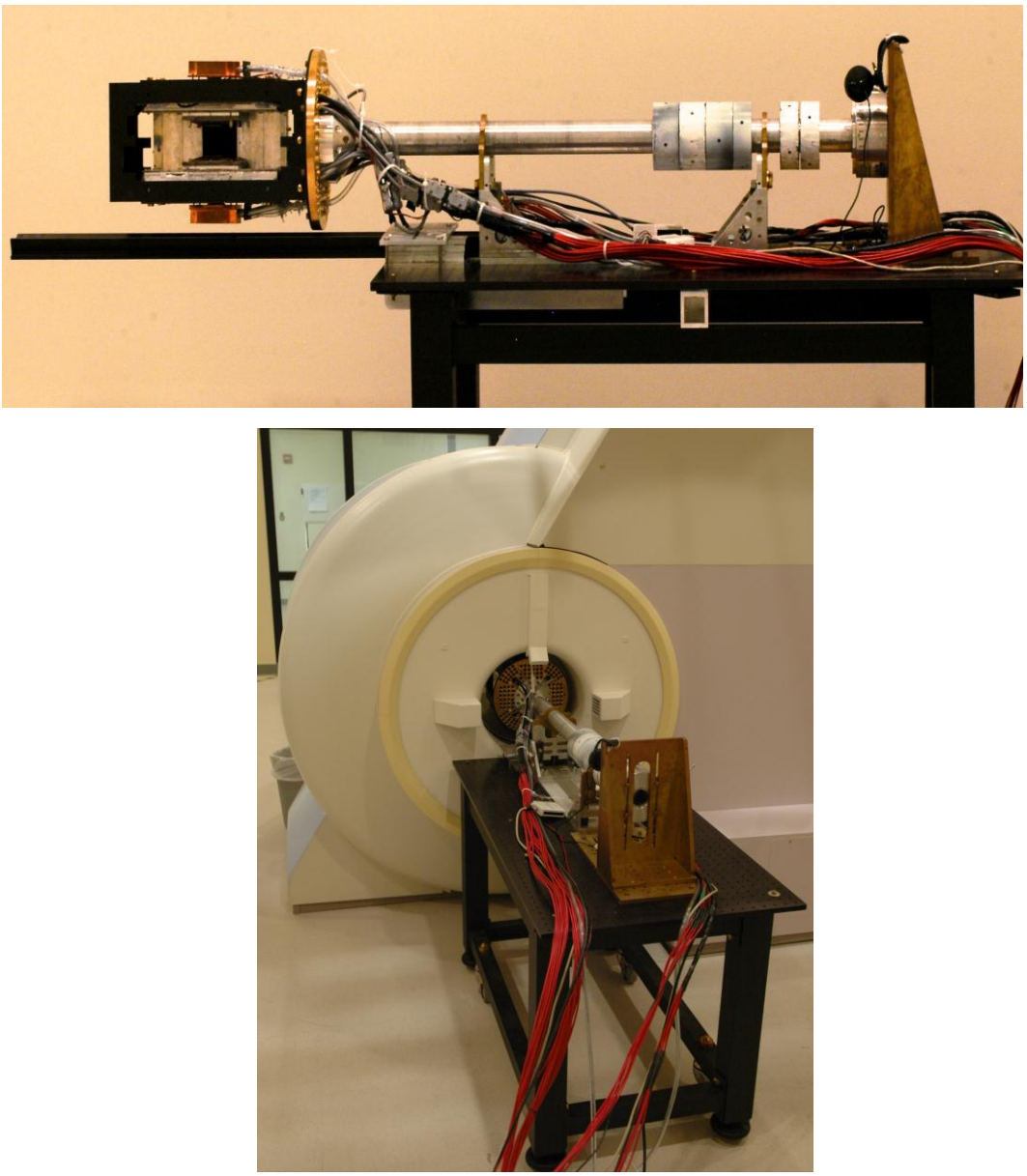

Fig. 6. The MR compatible SPECT system (Upper: portable SPECT system on a MR safe cart; Lower: SPECT cameras inside a 3T scanner)

CHAPTER 3. INTRINSIC PERFORMANCE OF ERPC DETECTORS

3.1 Experimental setup

In order to evaluate the performance of the ERPC detector, we constructed a fine-beam collimator as shown in Fig. 7. The collimator consists of four pieces of tungsten that are attacked together to create a narrow channel with a cross-section area of 100 μm×100 μm in size and a total length of 1.2 cm. A Co-57 point source of 250 μm diameter is attached to one end of the channel. The collimator/source assembly is attached to a precise x-y stage through a goniometer that allows the angle of incidence to vary from 0 to 65 degrees.

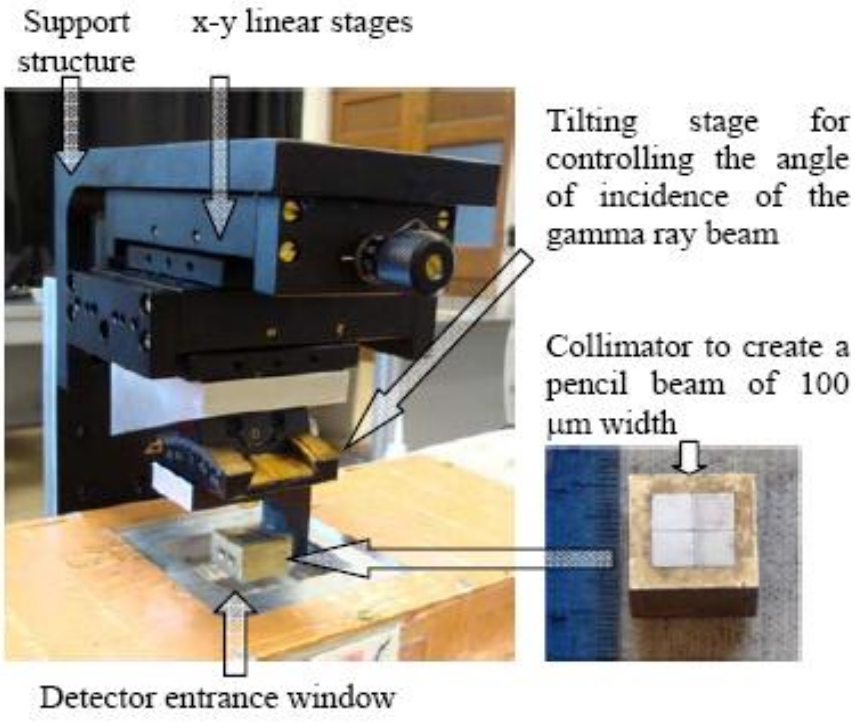

Fig. 7. Experimental setup for illuminating the detector with a fine pencil-beam.

In this study, we fine-tuned the angle of incidence for the Co-57 gamma ray beam and the point of incidence to create interactions happened roughly below a fixed pixel. By scanning

the setup parallel to the surface of the detector, the depth-of-interaction is changed through the 1 mm thickness of the detector.

3.2 Energy resolution

As mentioned above, we investigated the energy resolution at different depth of a single pixel using pencil beam Co-57 source. The energy resolution achieved is around 3kev for the 1mm CdTe detector as shown on Fig. 8. The energy resolution of the 2mm CdTe is a little lower than that of 1mm detector. The comparison of energy resolution of 1mm/2mm CdTe detectors is shown on Fig. 9.

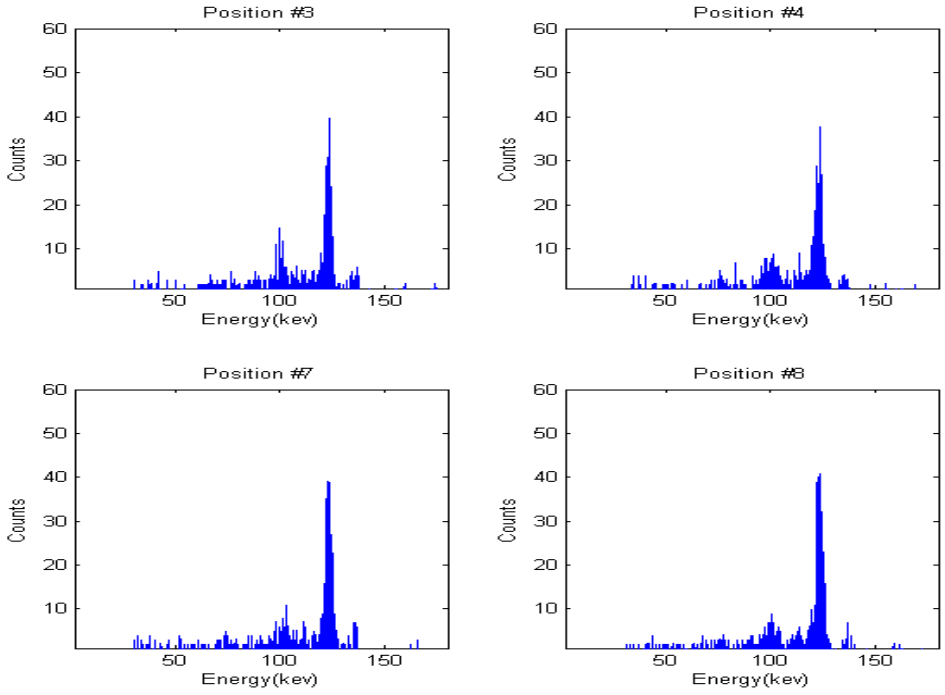

Fig. 8 Energy spectra measured on a single pixel with events at different depths-of-interaction.

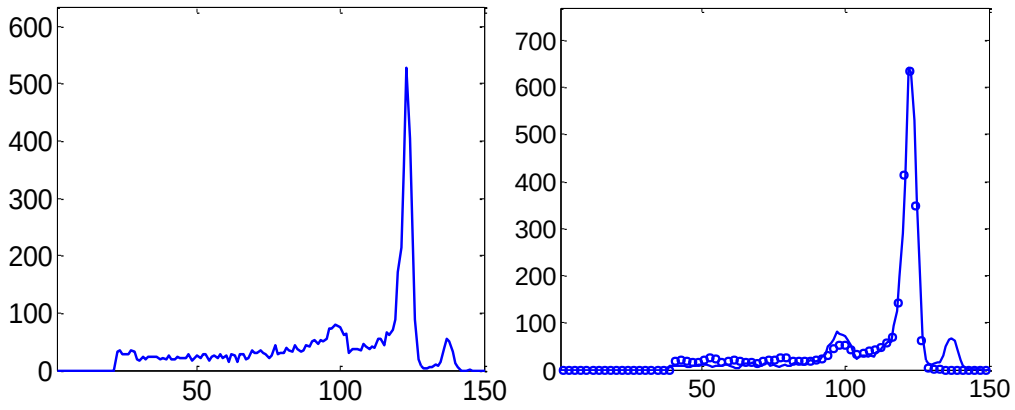

Fig. 9. Energy resolution measured on single pixel of 1mm/2mm CdTe ERPC detector (Left: 1mm CdTe, E.R=3.51kev; Right: 2mm CdTe, E.R=4.62kev;).

3.3 Detector uniformity

Fig. 8 and Fig. 9 show the energy resolution of the ERPC detectors. The energy resolution in individual pixels is around 3~4 kev. In this study, we also evaluated the

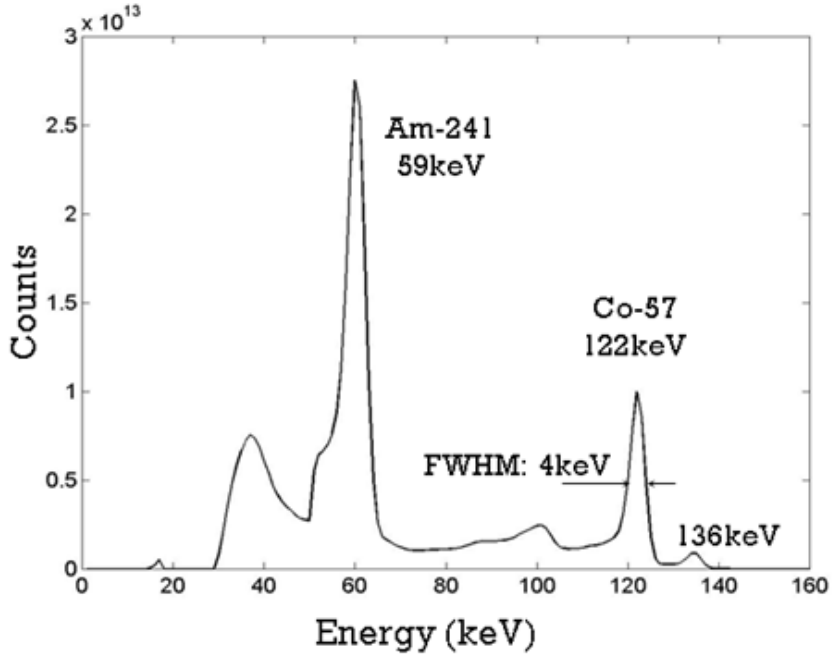

Fig. 10. Energy spectrum with events acquired on all 16384 pixels after correcting the channel-by-channel variation of gain and offset

uniformity of the current ERPC detector with the flood illumination geometry. The full-energy peak positions for Co-57 and Am-241 gamma rays were used to determine the gain and offset values for each of the 16384 pixels (Fig. 10). The distribution of pixel-wise gain and offset values are shown in Fig. 11, which demonstrated a relative uniform response of the detector over the 128×128 pixels. There are less than 0.5% of pixels on the current detector that exhibited very low gain and therefore marked as the dead pixels.

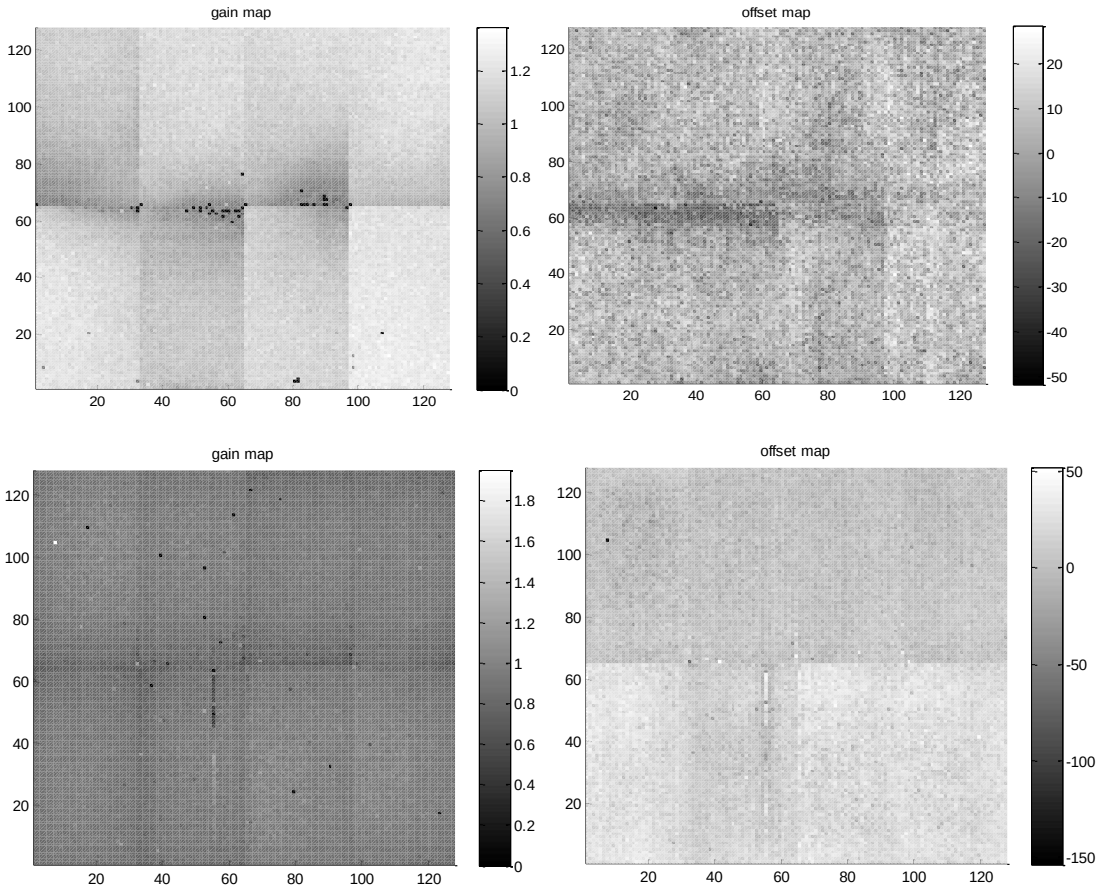

Fig. 11. The distribution of channel gain values across 16384 detector pixels. Dead pixels are <0.5% on the CdTe detectors. (The upper two figures demonstrate the gain and offset map of the 1mm CdTe ERPC detector, the lower two figures show the gain and offset map of the 2mm CdTe ERPC detector.)

CHAPTER 4. DEVELOPMENT AND EVALUATION OF SPECT IMAGING

4.1 Geometry calibration of SPECT system

An accurate geometrical calibration is of great importance for achieving SPECT image with high spatial resolution. Geometrical parameters required for system modeling were obtained based on a calibration process that we have previously developed for an ultrahigh resolution SPECT system [14]. With this method, a spherical Co-57 source of 250 μm is supported on a linear translation stage that can move the source along the axis of the object. At each axial stage, the detection system can be rotated at arbitrary steps to record the corresponding projections. The accumulation process is controlled by a Labview user interface. Parameters such as rotation steps, accumulation time for each step can be set friendly in the user interface. For each camera heads, there are 65 parameters defined to account for the geometry. The rotation axis is defined as a global X axis. 2 parameters are used to present the initial position of calibration point source in the Y-Z plane (assume that the initial position of the calibration point source in the X axis is zero). 6 parameters are used to provide the center position and surface direction of the detector. We also define 3 parameters to consider the angle between the rotation axis and the linear translation direction. Besides these 11 parameters mentioned above, each pinhole is corresponding to another 6 parameters which account for the pinhole space position and direction. At each angle, by processing the projection through the 9 pinholes, we can calculate the centroid of projection through each pinhole and use these centroid information to do geometrical calibration [14]. The comparison of experimental and calibrated centroid is shown on Fig. 12 and an example

projection on one particular angel is shown on Fig. 13.

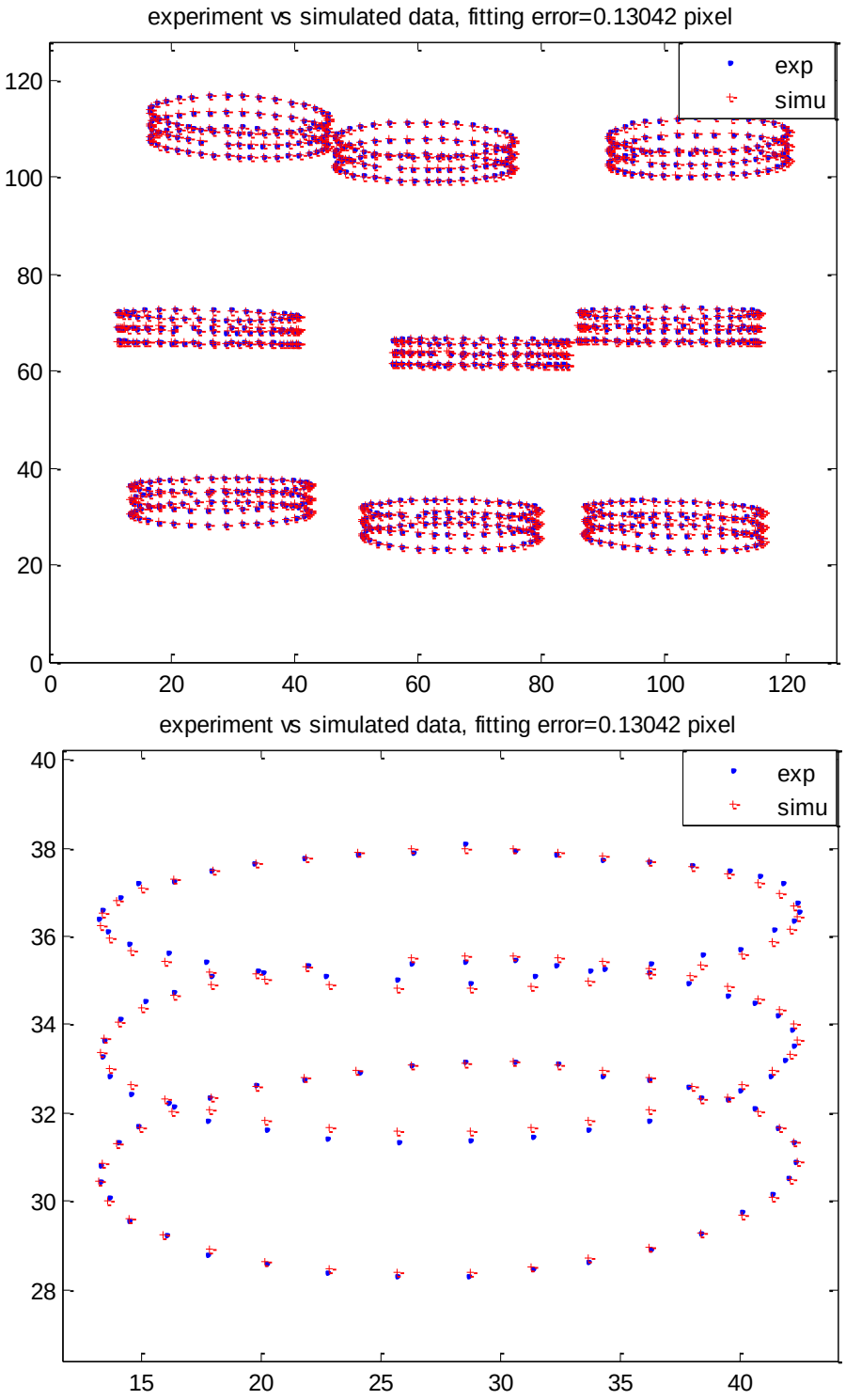

Fig. 12. Experimental projection centroid and calibrated projection centroid comparison, the lower is the zoomed centroid comparison through one pinhole (The 0.1342 pixel is the average experimental and calibrated centroid error)

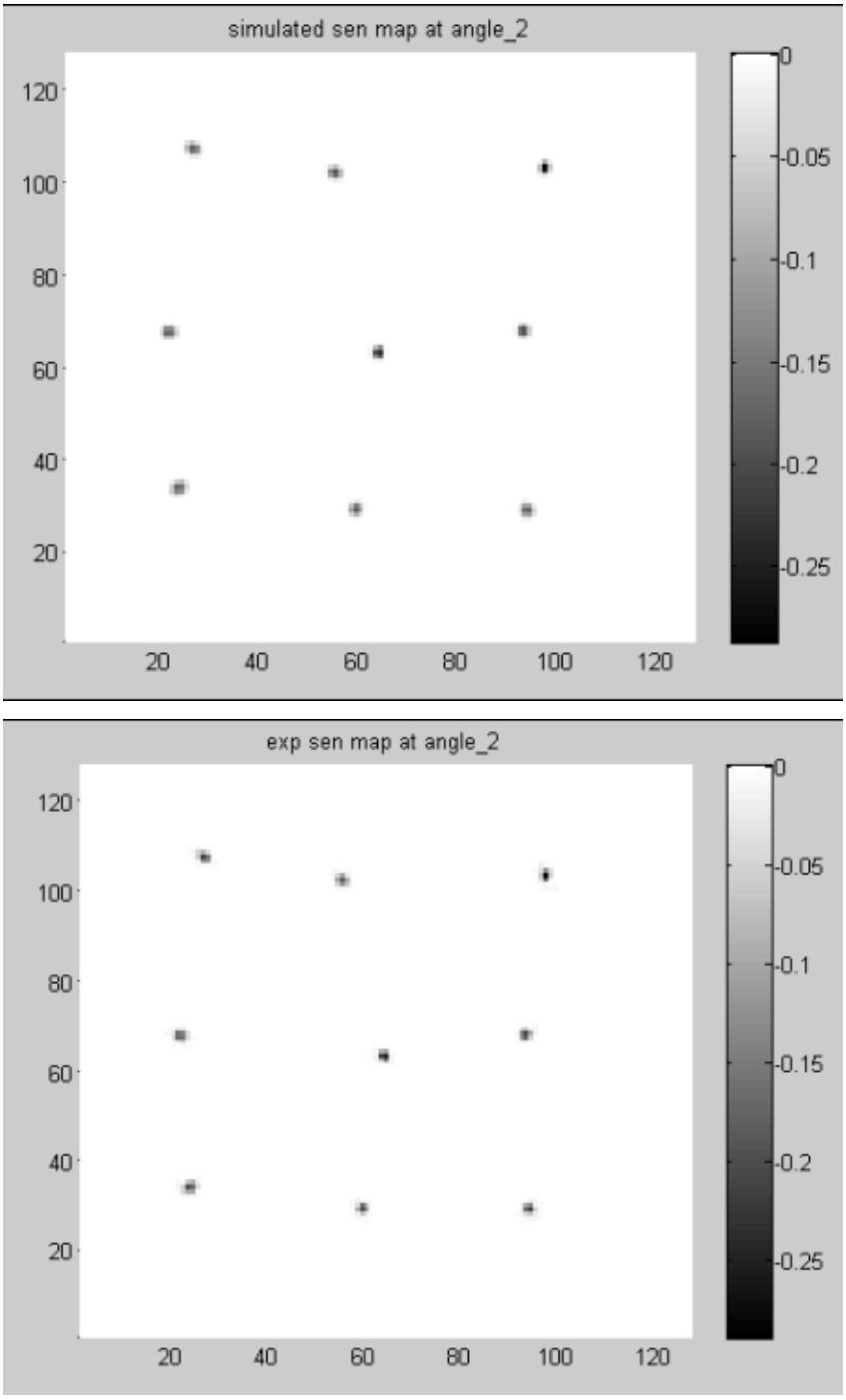

Fig. 13. The experimental and calibrated projections at a particular angle. (For each pinhole projection, the experimental and calibrated probabilities have been normalized)

To better account for detailed physical response of the system, we further refined the

previous calibration process. Firstly, in the previous method, only the centroid of point-source projections were used in weighted least-square (WLS) fitting process for finding the model parameters. For 140 keV gamma rays, the penetration of the photons in detector could lead to projections of asymmetric shape. By contrast, the current fitting process uses the entire projected profile in the WLS fitting. This helps to account for physical factors, such as the depth-of-interaction effect in detector and the complicated pinhole geometry. Secondly, for the new calibration routine, the trajectory of point source is designed to cover the entire object space. This is implemented by scanning the point source through a larger number of axial and trans-axial positions. This process helps to determine the uniformity of the system response and to assess the accuracy of the predicted

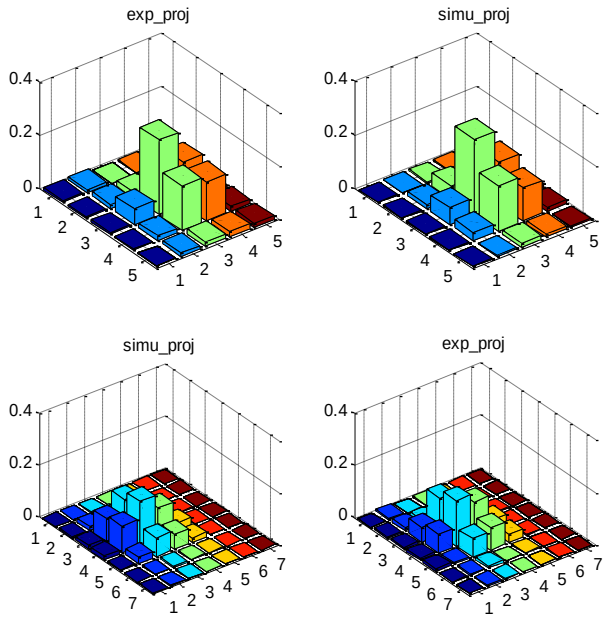

Fig. 14 the experimental and modeled projection profile through single pinhole on detectors after geometrical calibration (the upper is the projection got from 200μm pinhole while the lower is got from the 400 μm pinhole).

system model. A comparison between measured and predicted projections through a single pinhole is shown on Fig. 14 and the projection process through multiple pinhole aperture can be seen at Fig. 15. At present, the average root-mean-square (RMS) distance between measured and predicted projection centers was around 50 μm. The calibration accuracy achieved with this fitting process should be adequate for the ERPC detector based SPECT system.

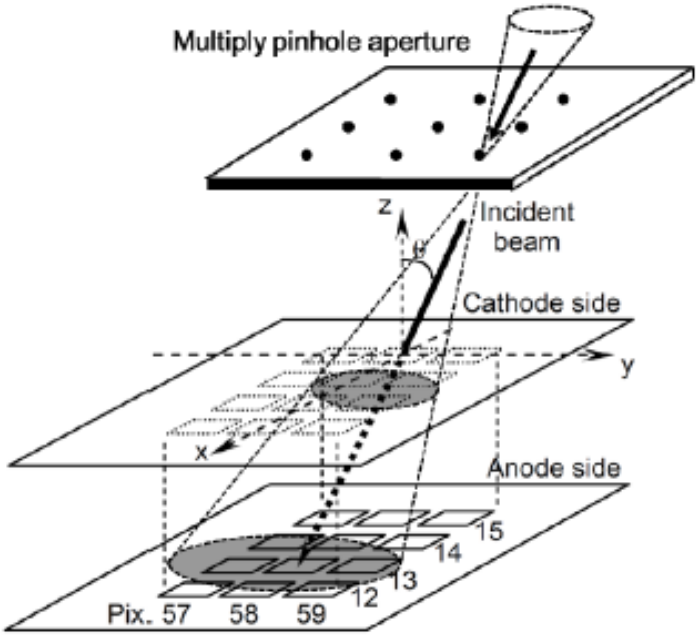

Fig. 15. Multiple pinhole projection model considering depth of interaction

4.2 System modeling and image reconstruction

4.2.1 System modeling

In order to model the complex pinhole geometry, we have developed a flexible simulation

package that could be adapted to arbitrary pinhole geometry. With this approach, the aperture is modelled as multiple layers of thin sheets having openings defined to mimic the actual pinhole geometry. For simplicity, the opening always has its sidewall perpendicular to the surface of the layer. Each layer could be defined with arbitrary material, which allows to the modeling of tungsten inserts placed inside through holes drilled through lead sheet. The overall attenuation of a gamma ray through the aperture could be derived based on the attenuation induced by all the layers. To further improve the accuracy, we can also model different layers with variable thickness – thinner layers could be used for sections close to the knife-edge of the pinhole. The advantage of this approach is that it allows one to model the photon penetration through almost any pinhole geometry. Given the amount computation involved, we typically pre-compute the model for each pinhole and store the resultant attenuation factors in memory. The expected attenuation for photons from a given pixel to a detector pixel is can be looked up on-the-fly during image reconstruction.

The system response function also includes the depth-of-interaction effect on pixilated CdTe detector. This is realized by modeling the detector as, in effect, 4-16 layers of independent detectors. Since 85% of 140 keV gamma rays will interact with CdTe through photoelectric effect, we ignored the possibility of a gamma ray Compton scattered in one layer and then stopped in another layer.

3-D image reconstruction was performed using a modified ordered-subset (OS) [15] penalized maximum-likelihood (ML) algorithm that also includes inter-iteration filtering to stabilizing the solution. This algorithm was combined with a non-uniform object-space pixelation scheme that we have recently developed for improving computation efficiency.

4.2.2 Evaluation of SPECT reconstruction image

To evaluate the spatial resolution of the dual-head SPECT system, a sealed Co-57 point source(~70 μCi) was used for the SPECT scan. The active element is a ceramic bead of 250 μm diameter. The aperture used here is with 3 by 3 pinhole pattern and the pinhole diameter is 200 μm. The field-of-view of the SPECT system is designed to be 1.5cm in diameter. In order to investigate the spatial resolution within different position inside the field-of-view, we scan the point source with different rotation radius, ranging from 1mm to 8mm. The reconstructed image of the point source within different rotation radius can be used to predict the resolution difference inside the field-of-view. For each radius, the point source is scanned for 16 angular steps and each step has 15 minutes accumulation time. Images are reconstructed with 60 μm voxel size using OS-EM algorithm using 180 iterations. Reconstruction results of point source at different positions are shown on Fig. 16 and Fig. 17. To quantify the spatial resolution, the full-width at half-maximum (FWHM) of the point source along the axial and trans-axial direction is calculated as shown in Fig. 18. The FWHM is measured from a least-squares fir of a Gaussian function to the line profile.

The spatial resolution of this SPECT system is also evaluate with the lab made phantom. This lab made miniaturized Jaszak phantom has a hot rod insert of 1.3 cm in diameter and around 5 mm in length. The insert has four groups of through holes parallel to the axis. The diameters for these holes are 1 mm, 0.75 mm, 0.5 mm and 0.35 mm respectively. Within each group, the minimum spacing between centers of two adjacent holes is two times their diameter. The phantom contains a total activity of around 3mCi. Fig. 19 shows the phantom images reconstructed. The projections were acquired with 60 angular steps and each

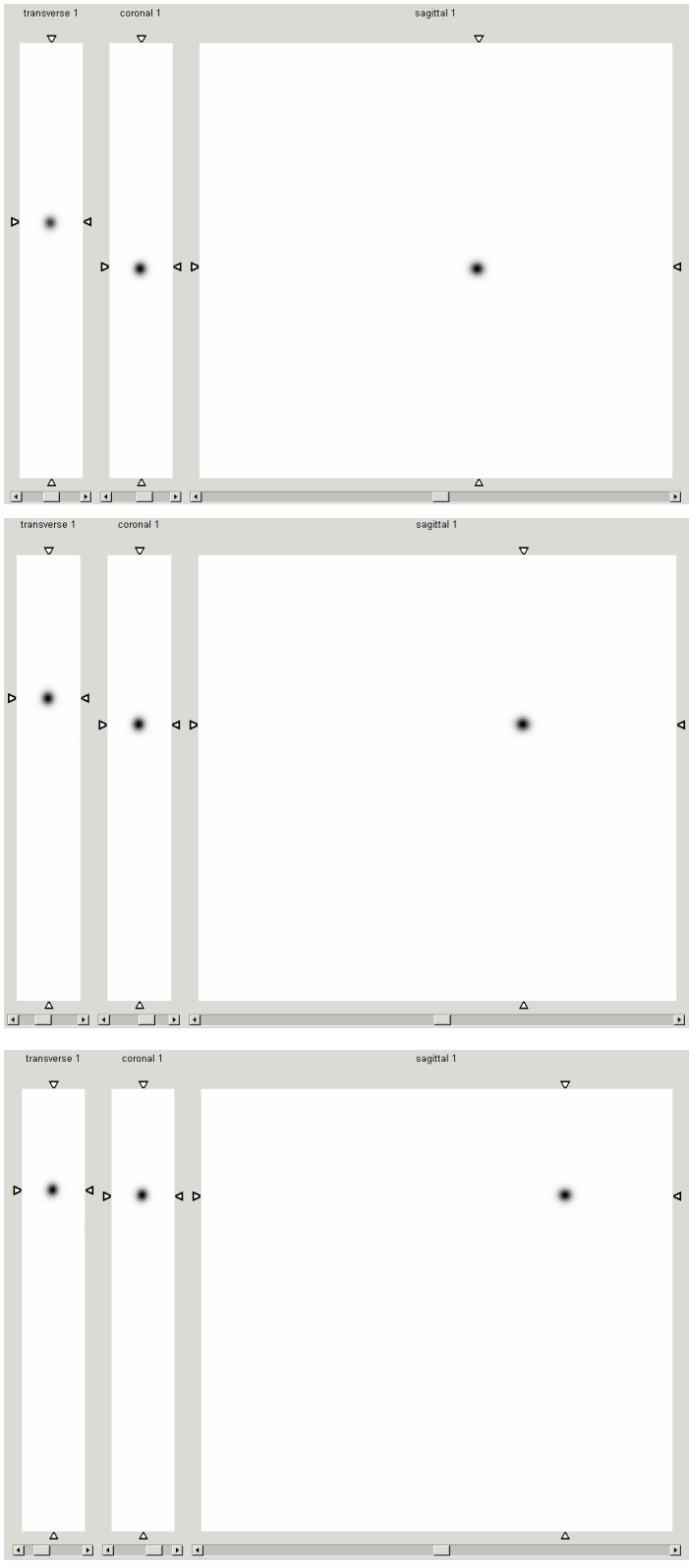

Fig. 16. Point source images at different position inside the field of view.
(Upper to lower: point source rotation radius of 1.6mm/4.6mm/7.6mm, respectively)

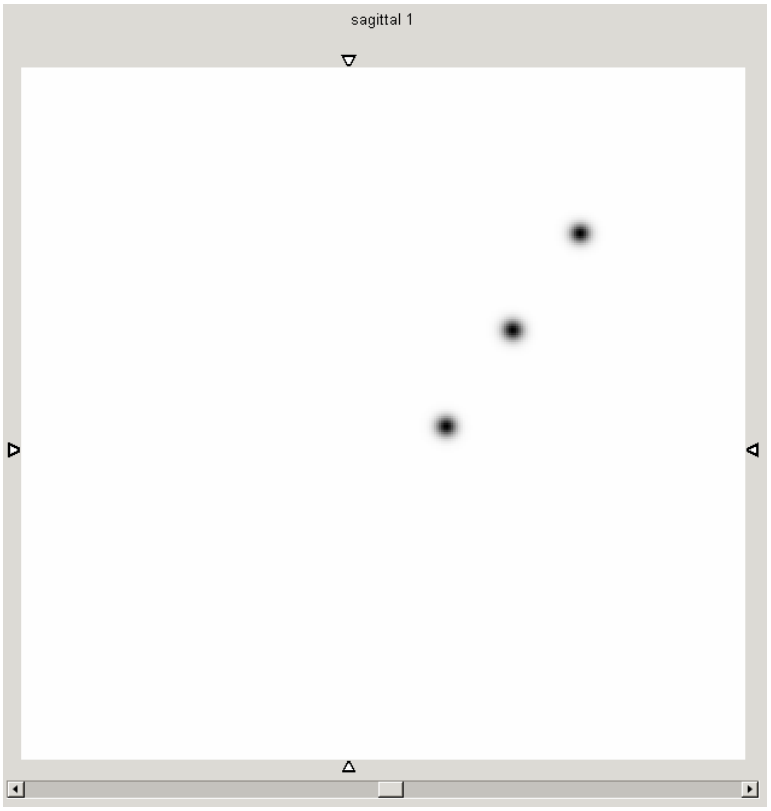

Fig.17. Sagittal cross-section of point source image at different position (radius from rotation axis 1.6mm/4.6mm/7/6mm)

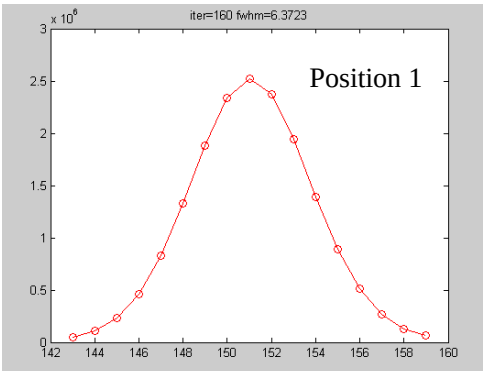

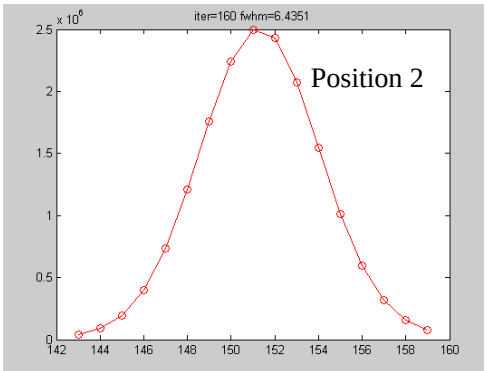

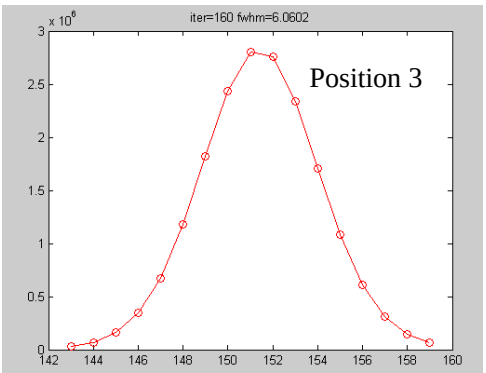

Fig. 18 The full-width at half-maximum (FWHM) of the point source along the trans-axial direction at different position. (voxel size is 60μm, and the FWHM is 382μm, 386μm and 364μm, respectively)

step has 6 minutes accumulation time. 106 iterations, four subsets and 0.25mm voxel size are used in the reconstruction process. The 500 μm features can be clearly resolved.

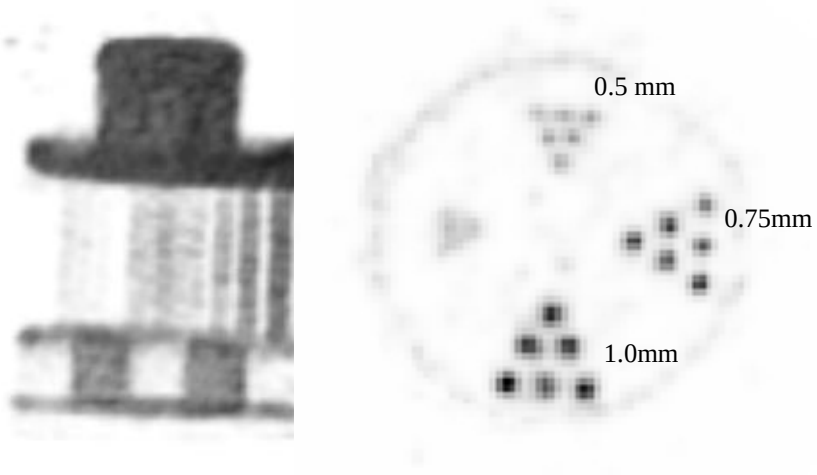

Fig. 19. Reconstructed phantom image, the 0.5mm feature is resolved clearly

4.3. MR correction and corresponding image

To investigate the SPECT imaging performance in strong magnetic field, the images of resolution phantom were obtained outside and inside 3T MRI scanner. With presence of magnetic field, there are image distortion and poor spatial resolution compared to the image taken outside MRI scanner as we predicted. To compensate for this obviously distortion caused by Lorenz force in strong magnetic field, a detailed charge collection model inside strong magnetic field has been developed in our group by J. W. Tan [16,17], A new system response function is generated to compensate for the MR shift effect and the detailed correction model can be seen in [17]. By using the newly refined system response function integrating the first-order correction for Lorenz force, the reconstructed image was compared

to the image outside MRI and the one inside MRI but without any correction in Figure 20. The comparison clearly demonstrated that the SPECT image with first-order effect considered has shown much improved image quality and better spatial resolution.

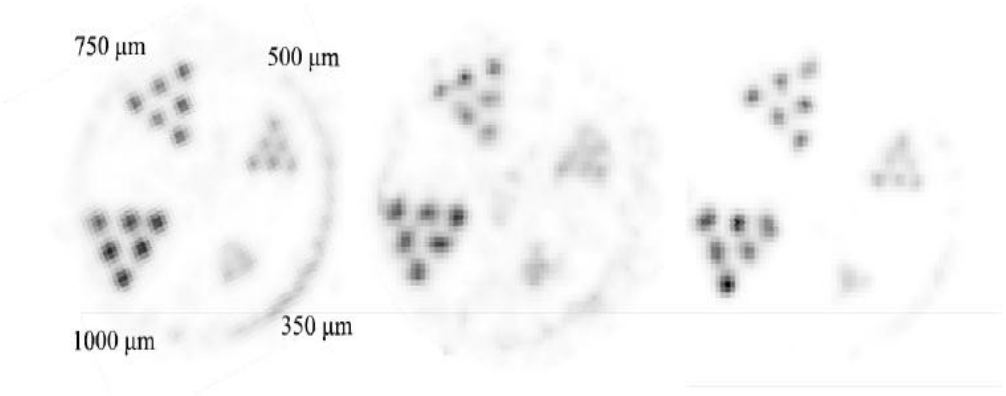

Fig. 20. (Left) SPECT Image of a micro-Jaszczak phantom outside the MR scanner; (Middle) SPECT image acquired inside the MR scanner without correction; (Right) SPECT image acquired inside the MR scanner with the first order correction.

CHAPTER 5. SUMMARY AND CONCLUSION

In this thesis, we have developed a prototype MR compatible SPECT system based on recently developed energy-resolved photon-counting CdTe detectors. The design of the ERPC detector offers an excellent intrinsic detector performance that includes an energy resolution of around 3~4 keV (at room-temperature), an excellent resolution of around 350 μm and a good charge collection efficiency for electron signal created by 140 keV gamma rays. In this study, we demonstrated the intrinsic performance of the CdTe ERPC detectors and experimentally evaluated the imaging performance of a four-head SPECT system. Both point source and laboratory made phantoms images are investigated. With the developed geometry calibration, system modeling as well as the reconstruction package, this prototype SPECT system is able to achieve sub-500μm spatial resolution. By using the charge collection model inside strong magnetic field developed by J. W. Tan, the SPECT image outside and inside MR is reconstructed and compared. The image improvement by using the correction model can be obviously seen. These have provided valuable insights in using the ERPC detectors for future simultaneous SPECT/MR studies.

CHAPTER 6. REFERENCE

[1] C. Catana, D. Procissi, Y. Wu, M. S. Judenhofer, J. Qi, B. J. Pichler, R. E. Jacobs, S. R. Cherry, "Simultaneous in vivo positron emission tomography and magnetic resonance imaging." *Proc. National Acad. Sci. USA* 105(10): 3705-3710 2008.

[2] N. Zhang, R. F. Grazioso, N. K. Doshi, and M. J. Schmand, "RF transformer coupled multiplexing circuits for APD PET detectors," *IEEE Trans. Nucl. Sci*., vol. 53, pp. 2570-2577, 2006.

[3] C. Woody, D. Schlyer, P. Vaska, D. Tomasi, S. Solis-Najera, W. Rooney, J. F. Pratte, S. Junnarkar, S. Stoll, Z. Master, M. Purschke, S. J. Park, S. Southekal, A. Kriplani, S. Krishnamoorthy, S. Maramraju, P. O'Connor, and V. Radeka, "Preliminary studies of a simultaneous PET/MRI scanner based on the RatCAP small animal tomograph," *Nucl. Instr. Methods A*, vol. 571, pp. 102-105, 2007.

[4] B. J. Pichler, M. S. Judenhofer, C. Catana, J. H. Walton, M. Kneilling, R. E. Nutt, S. B. Siegel, C. D. Claussen, and S. R. Cherry, "Performance test of an LSO-APD detector in a 7-T MRI scanner for simultaneous PET/MRI," *Journal of Nucl Med*, vol. 47, pp. 639-647, 2006.

[5] E. Breton, P. Choquet, C. Goetz, J. Kintz, P. Erbs, R. Rooke, and A. Constantinesco, "Dual SPECT/MR imaging in small animal," *Nucl. Instr. Methods A*, 571(1-2): 446-448, 2007.

[6] C. Goetz, E. Breton, P. Choquet, V. Israel-Jost, and A. Constantinesco, "SPECT low-field MRI system for smallanimal imaging," *Journal of Nucl. Med* 49(1): 88-93, 2008.

[7] S. R. Meikle, et al., "Small animal SPECT and its place in the matrix of molecular imaging technologies," *Physics in Medicine and Biology*, vol. 50, pp. R45-R61, Nov 21 2005.

[8] C. S. Levin, “Small animal PET and SPECT: Instrumentation, performance, and applications,” *Medical Physics*, vol. 32, pp. 2096-2096, Jun 2005.

[9] S. R. Cherry, “In vivo molecular and genomic imaging: new challenges for imaging physics,” *Physics in Medicine and Biology*, vol. 49, pp. R13-R48, Feb 7 2004.

[10] F. van der Have, et al., “U-SPECT-II: An Ultra-High-Resolution Device for Molecular Small-Animal Imaging,” *Journal of Nuclear Medicine*, vol. 50, pp. 599-605, Apr 1 2009.

[11] F. J. Beekman, et al., “U-SPECT-I: A novel system for submillimeter-resolution tomography with radiolabeled molecules in mice,” *Journal of Nuclear Medicine*, vol. 46, pp. 1194-1200, Jul 2005.

[12] H. H. Barrett, Lars R. Furenlid, Melanie Freed, Jacob Y., Hesterman, Matthew A. Kupinski, Eric Clarkson, and Meredith K. Whitaker, “Adaptive SPECT,” *IEEE Transactions on Medical Imaging*, vol. 27, no. 6, June 2008

[13] L. J. Meng, J. W. Tan, K., Spartiotis, T. Schulman, “Preliminary evaluation of a novel energy-resolved photon-counting gamma ray detector,” *Nucl. Instr. Methods A*, 604(3): 548-554. 2009.

[14] L. J. Meng, and G. Fu, “An ultrahigh resolution SPECT system for I-125 mouse brain image studies.” *Nucl. Instr. Methods*, 600(2), pp. 498-505, 2009.

[15] H. M. Hudson and R. S. Larkin, “Accelerated Image-Reconstruction Using Ordered Subsets of Projection Data,” *IEEE Trans. Med. Imaging*, vol. 13, pp. 601-609, 1994.

[16] J. W. Tan, L. Cai., and L. J. Meng, “A prototype of the MRI compatible ultra-high resolution SPECT for in vivo mice brain imaging,” *IEEE Nucl. Sci. Symp, and Med. Imag. Conf*, 2800-2805, 2009.

[17] J. W. Tan, L. Cai and L. J. Meng, “Experimental Study of the Response of 1-5 mm Thick CdTe/CZT Detectors inside Strong Magnetic Field,” *IEEE Nucl. Sci. Symp, and Med. Imag. Conf*, 2010.

AUTHOR'S BIOGRAPHY

Liang Cai got his bachelor's degree in Department of Modern Physics in University of Science and Technology of China in 2008. After graduation, he joined the Department of Nuclear, Plasma and Radiological Engineering at University of Illinois at Urbana-Champaign to start his graduate study. After one year's teaching assistant experience, he joined the Radiation Detection and Imaging group and focused his research on medical imaging. Currently he is working on a DOE funded project as mentioned in this thesis. Following the completion of his Master degree, he will continue his research on this MR-compatible SPECT project and pursue a Ph.D. degree.